Dynamic analysis and optimization of a novel reconfigurable parallel mechanism

Guanyu Huang
Zhejiang Lab
Dan Zhang (dzhang99@yorku.ca)
York University https://orcid.org/0000-0002-7295-4837
Qi Zou
York University
Ling-Yu Kong
Zhejiang Lab

Research Article

Keywords: over-constrained mechanism, reconfigurable parallel mechanism, dynamic and kinematic analysis, dynamic model, optimization

Posted Date: March 29th, 2022

DOI: https://doi.org/10.21203/rs.3.rs-1438927/v1

Title page

Dynamic analysis and optimization of a novel reconfigurable parallel mechanism

Guan-Yu Huang, born in 1989, is an assistant researcher in *Zhejiang Lab, China.* He received his Bachelor's and PhD degrees from *Beijing Jiaotong University* in 2013 and 2018 respectively. His research interests include design and control of parallel, biped and other robots.
E-mail: huanggy@zhejianglab.com

Dan Zhang, received his Ph.D. in Mechanical Engineering from *Laval University*, Canada, in June 2000. His research interests include robotics and mechatronics; high performance parallel robotic machine development; sustainable/green manufacturing systems; rehabilitation robot and rescue robot. Dr. Zhang's contributions to and leadership within the field of robotic and automation have been recognized with several prestigious awards, within his own university (Kaneff Professorship, Tier 1 York Research Chair in Advanced Robotics and Mechatronics, Research Excellence Award), the Province of Ontario (Early Researcher Award in 2010), the professional societies (Fellow of the Canadian Academy of Engineering, Fellow of the ASME, Fellow of the Engineering Institute of Canada and Fellow of the CSME, Senior Member of IEEE, Senior Member of SME), and federal funding agencies (Canada Research Chair in January 2009 and renewed in January 2014).
E-mail：dzhang99@yorku.ca

Qi Zou, received his Bachelor's and Master's degrees from *Beijing Jiaotong University* in 2016 and 2019, respectively. Currently he is a doctoral student in Mechanical Engineering at *York University*. His research interests contain design and performance analysis of parallel mechanism.
E-mail: qizou@yorku.ca

Ling-Yu Kong, born in 1988, is currently a researcher at *Intelligent Robot Research Center, Zhejiang Lab*, Hangzhou, China. He received his PhD degree from *Shanghai Jiao Tong University*, China in 2018. His research interests include mechatronics engineering, robotics and manipulator calibration.
E-mail: kongly@zhejianglab.com

Corresponding author：Dan Zhang　E-mail：dzhang99@yorku.ca

ORIGINAL ARTICLE

Dynamic analysis and optimization of a novel reconfigurable parallel mechanism

Guan-Yu Huang[1, 2] • Dan Zhang[2*] • Qi Zou[2] • Ling-Yu Kong[1]

Abstract: In this paper, a new reconfigurable parallel mechanism by applying a spatial multi-loop over-constrained mechanism is proposed. The reconfigurable parallel mechanism has 4 degrees of freedom (DOF), and its different performance indices can be continuously changed. According to its inverse kinematic model, its workspace, dexterity, and stiffness are all analyzed. This paper also establishes the dynamics model, and a novel dynamic index is proposed to optimize the proposed mechanism. With these novel performance indices, both the kinematic and the dynamic performance for this mechanism are shown to be greatly improved.

Keywords: over-constrained mechanism • reconfigurable parallel mechanism • dynamic and kinematic analysis • dynamic model • optimization

1 Introduction

In recent years, much research has focused on parallel mechanisms with reconfigurable abilities. This is because these mechanisms have advantages over parallel mechanisms or reconfigurable mechanisms[1, 2]. Based on their structural characteristics, reconfigurable parallel mechanisms have not only high accuracy and stiffness, but also the ability to change their structural parameters, which can reach a different performance to adapt to different industry tasks[3-5]. Reconfigurable parallel mechanisms are widely used in 3D printers[6], surgery[7], machine tools[8, 9], and other areas.

To obtain different types of reconfigurable parallel mechanisms, researchers have proposed several approaches for designing reconfigurable parallel mechanisms. In consideration of reconfigurable limb structure and of using a metamorphic linkage, Ye et al.[6, 10, 11] proposed a class of parallel mechanisms that are reconfigurable. By locking or releasing some joints, the metamorphic limbs were configured to a five-bar limb, diamond limb, and a hybrid limb. By applying a spatial hybrid mechanism, Zhang et al.[12] designed a parallel mechanism that can change its type of its degree of freedom (DOF). And this mechanism can change itself from a 3-DOF spherical mechanism to a 1-DOF, translational parallel mechanism. Similarly, several novel joints have been proposed to obtain reconfigurable parallel mechanisms. Gan et al.[13-15] designed a novel reconfigurable joint, which can give the parallel mechanism the capability to change its configurations. These joints can change the type of mobility, such as from rotation to translation, by changing the directions of their axes.

Dynamics analysis is significant for industrial application of parallel mechanisms. By applying different mechanical principles, several dynamics methods have been presented to calculate the dynamic model. By using Newton's and Euler's dynamic equation, a Newton-Euler method has been presented to derive the dynamics model of a mechanism considering the internal and external force.[16-19] For a 3 DOFs parallel mechanism with a passive limb, Zhang et al.[16] employed the Newton–Euler method to establish its inverse dynamic model, and an example was proposed to verify the concept of the new design proposed in this paper. Wu et al.[19] applied the Newton-Euler method to deal with the inverse dynamic model for a 2 DOFs mechanism. Compared with Newton-Euler's law, the virtual work method is one more efficient method for analyzing the dynamic model for a parallel mechanism[20]; much research[21-24] has used

✉ Dan Zhang
dzhang99@yorku.ca
[1] Zhejiang Lab, 1818 Wenyi West Road, Hangzhou, 311121, China
[2] Department of Mechanical Engineering, Lassonde School of Engineering, York University, 4700 Keele Street, Toronto, ON M3J 1P3, Canada

this method. To collect solar energy, Wu et al.[23] proposed a novel, two-axis, decoupled mechanism, and the dynamic model for this parallel mechanism was conducted using the virtual work principle. For a 3-DOF redundancy parallel mechanism, Wu et al.[24] also solved the inverse dynamic model by applying virtual work principle. At the same time, the force of actuators was optimized by applying the least-square method. Staicu et al.[21] presented a novel method to establish the kinematic model - called the recursive matrix method - with the kinematics model; the virtual work's principle was applied to derive a 3 DOFs parallel mechanism's dynamics model. The Lagrangian formulation is also an efficiency method for solving the dynamics problem, because of the elimination of initial forces and moments, especially for three-translation parallel mechanisms[20]. Much research has been done based on this approach[25-28]. For the 4-UPS-UPU parallel mechanism, Chen et al.[28] established a nonlinear, elastic dynamics model by applying the Lagrange method. Then, its dynamic response was analyzed, and the chaos phenomenon contained in the mechanism was identified by phase diagrams. Yao et al.[26] applied the Lagrangian equation to calculate the dynamic model for a 5-DOF, redundant parallel mechanism.

Optimization for parallel mechanisms is a key step in designing industrial robots[29]. Some researchers have studied the optimum design of parallel mechanisms.[30-35] Based on an optimization algorithm, Gao et al.[30] investigated optimization for a serial-parallel hybrid machine tool and presented some local and global indices. Zhang et al.[35] proposed a novel performance index to optimize a mechanism. Considering the dexterous stiffness and other performance indices, they proposed a multi-objective optimization for this manipulator by using the particle swarm algorithm. Liu et al.[33] proposed one novel optimal kinematic design method, which they referred to as a performance, chart-based design methodology for parallel mechanisms with fewer than five linear parameters. In the case of translational parallel mechanisms, Zou et al.[36] optimized their workspace, dexterity, payload, and motion/force transmission index.

However, existing reconfigurable parallel mechanisms do not have the ability to change their configuration continuously, because they need to assemble different components to form the different configurations, or need to process the singularity position. At the same time, the optimization for reconfigurable mechanism mostly focuses on kinematic performance, while less attention is paid to dynamic performance. Dynamic performance is as important as the kinematics index in industrial applications. In this case, the two aspects limit the application areas of reconfigurable parallel mechanisms.

This paper proposes a new, reconfigurable parallel mechanism and it can be continuously reconfigurable and avoids singularity positions. Based on structural characteristics, the inverse dynamics model is calculated applying the Lagrangian method. According to the dynamics model, we propose a new dynamic performance index to optimize the proposed mechanism.

By using the spatial multi-loop over-constrained mechanism, a novel reconfigurable parallel mechanism is proposed, and in Section 2, its mobility is calculated. The kinematics and some numerical examples are investigated in Section 3. In Section 4, the dynamic models both for an over-constrained spatial multi-loop mechanism and parallel mechanism are analyzed, and a new dynamic performance is presented. Finally, the optimization design for the reconfigurable parallel mechanism is proposed.

2 Model description

The proposed reconfigurable parallel mechanism is assembled in two sections - one is the reconfigurable section, and the other is the parallel mechanism. In Figure 1, this mechanism is shown to have the fixed, the middle platform and the moving platforms. Between the middle and the fixed platforms, there are three identical limbs to connect these platforms. This section is the reconfigurable section, which is able to change the mechanism's structure between the minimum and maximum angles continuously. Similarly to the reconfigurable section, the parallel section has three limbs connecting the middle and moving platforms as well. This section also has three limbs which include prismatic joints, revolute joints, four-bar mechanisms, and revolute joints. By adjusting its reconfigurable part, the parallel section's structural parameters can be changed.

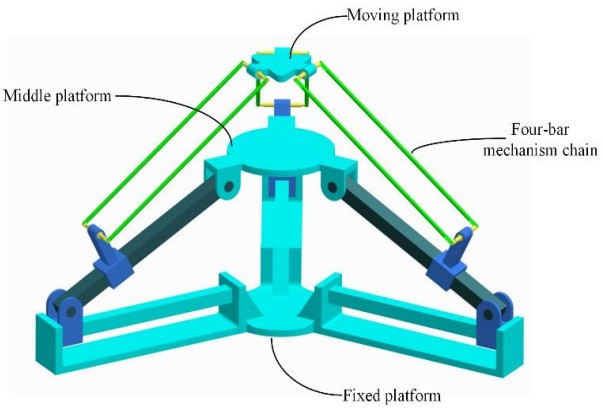

Figure 1 The proposed mechanism CAD model

Figure 2 shows the reconfigurable section of the proposed mechanism. By using over-constrained mechanisms, the designed mechanism is parallel type, as well. The proposed mechanism has three same limbs, but there are not three DOFs. According to screw theory, the mobility of the reconfigurable section can be analyzed[37].

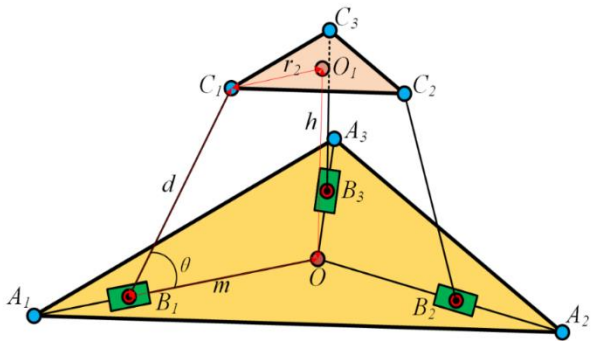

Figure 2 The over-constrained mechanism

The coordinates of $C_i(i=1,2,3)$ and $B_i(i=1,2,3)$ are denoted as $[x_{ci} \quad y_{ci} \quad z_{ci}]^{\mathbf{T}}$ and $[x_{bi} \quad y_{bi} \quad z_{bi}]^{\mathbf{T}}$, respectively. Thus, this limb's twist system (A_iB_i) can be given as follows:

$$\$_i = \begin{cases} & [0 \quad 0 \quad 0; \quad -a_i \quad b_i \quad 0]^{\mathbf{T}} \\ [b_i \quad a_i \quad 0; & -a_i z_{bi} \quad -b_i z_{bi} \quad -a_i z_{bi} + b_i y_{bi}]^{\mathbf{T}} \\ [b_i \quad a_i \quad 0; & -a_i z_{ci} \quad -b_i z_{ci} \quad -a_i z_{ci} + b_i y_{ci}]^{\mathbf{T}} \end{cases} (i=1,2,3) \tag{1}$$

where a_i and b_i are the axes directions of the ith joint.

And so, this limb's wrench system is obtained as:

$$\$_i^r = \begin{cases} \left[\dfrac{b_i}{a_i} \quad 1 \quad 0; \quad 0 \quad 0 \quad 0\right]^{\mathbf{T}} \\ [0 \quad 0 \quad 0; \quad 0 \quad 0 \quad 1]^{\mathbf{T}} \\ \left[0 \quad 0 \quad 0; \quad -\dfrac{b_i}{a_i} \quad 1 \quad 0\right]^{\mathbf{T}} \end{cases} (i=1,2,3) \tag{2}$$

Based on Eq.(2), the reconfigurable mechanism's twist system is written as:

$$\$ = [0 \quad 0 \quad 0; \quad 0 \quad 0 \quad 1]^{\mathbf{T}} \tag{3}$$

while the DOF of the reconfigurable mechanism is 1 - i.e., the translation along the z-axis.

For the parallel section, a simplified schematic diagram is shown in . Similarly to that of the reconfigurable section, the mobility for the parallel section can be analyzed as follows. The points E_i and F_i are denoted as $[x_{Ei} \quad y_{Ei} \quad z_{Ei}]^{\mathbf{T}}$ and $[x_{Fi} \quad y_{Fi} \quad z_{Fi}]^{\mathbf{T}}$. Thus, the parallel section's limbs are identical, and the twist system of this limb D_iF_i is written as:

$$\$_i = \begin{cases} [0 \quad 0 \quad 0; \quad l_i \quad m_i \quad n_i]^{\mathbf{T}} \\ [-m_i \quad l_i \quad 0; \quad l_i z_{Ei} \quad m_i z_{Ei} \quad -l_i x_{Ei} - m_i y_{Ei}]^{\mathbf{T}} \\ [a_i \quad b_i \quad c_i; \quad -c_i y_{Ei} + b_i z_{Ei} \quad c_i x_{Ei} - a_i z_{Ei} \quad -b_i x_{Ei} + a_i y_{Ei}]^{\mathbf{T}} \\ [a_i \quad b_i \quad c_i; \quad -c_i y_{Ei} + b_i z_{Ei} \quad c_i x_{Ei} - a_i z_{Ei} \quad -b_i x_{Ei} + a_i y_{Ei}]^{\mathbf{T}} \\ [a_i \quad b_i \quad c_i; \quad -c_i y_{Fi} + b_i z_{Fi} \quad c_i x_{Fi} - a_i z_{Fi} \quad -b_i x_{Fi} + a_i y_{Fi}]^{\mathbf{T}} \\ [a_i \quad b_i \quad c_i; \quad -c_i y_{Fi} + b_i z_{Fi} \quad c_i x_{Fi} - a_i z_{Fi} \quad -b_i x_{Fi} + a_i y_{Fi}]^{\mathbf{T}} \\ [-m_i \quad l_i \quad 0; \quad l_i z_{Fi} \quad m_i z_{Fi} \quad -l_i x_{Fi} - m_i y_{Fi}]^{\mathbf{T}} \end{cases} (i=1,2,3) \tag{4}$$

where l_i, m_i, n_i, a_i, b_i, and c_i are the directions of the prismatic and revolute joint axes.

Thus, the wrench system can be calculated as:

$$\$_i^r = \left[0 \quad 0 \quad 0; \quad -\frac{c_i l_i}{a_i l_i + b_i m_i} \quad -\frac{c_i m_i}{a_i l_i + b_i m_i} \quad l_i\right]^{\mathbf{T}} (i=1,2,3) \tag{5}$$

Based on Eq. (5), the parallel section's twist system is written as:

$$\$ = \begin{cases} [0 \quad 0 \quad 0; \quad 0 \quad 0 \quad 1]^{\mathbf{T}} \\ [0 \quad 0 \quad 0; \quad 0 \quad 1 \quad 0]^{\mathbf{T}} \\ [0 \quad 0 \quad 0; \quad 1 \quad 0 \quad 0]^{\mathbf{T}} \end{cases} \tag{6}$$

Based on Eq. (6), the parallel section has three translations, the proposed mechanism needs four actuators to make it work properly, and the moving platform possesses three translations along the three coordinate axes.

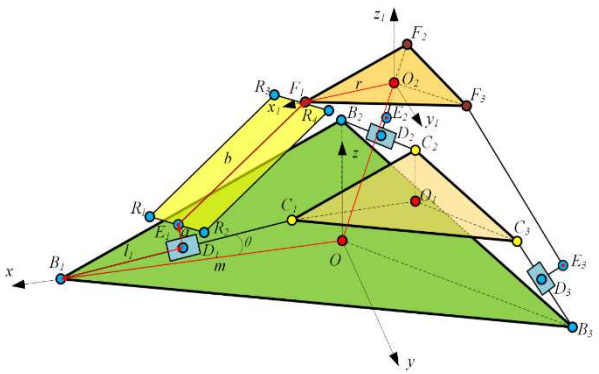

Figure 3 Schematic diagram of the parallel section

3 Kinematics analysis

3.1 Inverse kinematics

The structural parameters are different when the

reconfigurable section is at a different configuration. From Figure 2, we can see that the closed-loop vector equation is obtained as:

$$\overrightarrow{OB_1}+\overrightarrow{B_1C_1}=\overrightarrow{OO_1}+\overrightarrow{O_1C_1} \tag{7}$$

and the mathematical relationship between z_r and m is given as:

$$z_r=\sqrt{d^2-(m-r_2)^2} \tag{8}$$

where d is the link's displacement, and the middle platform's radius is denoted as r_2.

Figure 3 shows the vector schematic of one limb of the parallel part. O is the original point located at the global coordinate system, and O_2 is the moving platform's central point. The inverse kinematics problem is derived to calculate the length of different driving joints.

In this paper, the structural parameters can be defined as:

1. l_i is the ith length of the prismatic joint;
2. b is the length of the virtual link between E_i and F_i;
3. r is the radius of the circumcircle of the moving platform;
4. $[x_1 \quad y_1 \quad z_1]^{\mathrm{T}}$ is the coordinate of O_2;
5. a is the displacement between the revolute joint and prismatic joint.

According to the geometrical constraints, the mathematical equation is written as:

$$\overrightarrow{OB_1}+\overrightarrow{B_1D_1}+\overrightarrow{D_1E_1}+\overrightarrow{E_1F_1}=\overrightarrow{OO_2}+\overrightarrow{O_2F_1} \tag{9}$$

Thus, according to the structural parameters, the vector of $\overrightarrow{OE_1}$ is calculated as:

$$\overrightarrow{OE_1}=[m-l_1\cos(\theta)+a\sin(\theta) \quad 0 \quad l_1\sin(\theta)+a\cos(\theta)]^{\mathrm{T}} \tag{10}$$

In the moving coordinate system, $F_1^{'}$ can be written as:

$$F_1^{'}=[x^{'}+r \quad y^{'} \quad z^{'}]^{\mathrm{T}} \tag{11}$$

The rotation matrix must be calculated and the relationship between the moving and fixed coordinate systems can be obtained. Thus, the kinematics model can be established. The moving platform has three translations. So, its rotation matrix is given as:

$$R=\begin{bmatrix}1 & 0 & 0\\ 0 & 1 & 0\\ 0 & 0 & 1\end{bmatrix} \tag{12}$$

and the coordinate of point F_1 is obtained in the fixed coordinate system, which is:

$$F_1=R\cdot F_1^{'}+O_2^{'} \tag{13}$$

Then, vector $\overrightarrow{O_2F_1}$ is written as:

$$\overrightarrow{O_2F_1}=[x+r \quad y \quad z]^{\mathrm{T}} \tag{14}$$

By applying the geometrical constraints of the proposed mechanism, the equation is derived as follows:

$$\left\|\overrightarrow{E_1F_1}\right\|=b \tag{15}$$

Substituting Eqs. (10) and (14) into Eq. (15), the driving length is calculated.

To verify the parallel section's kinematic model, the desired moving platform's trajectory can be planned according to the industrial application. Assuming the industrial application is to mill a circular arc in a certain plane, the equation of the curve is set as:

$$\begin{cases}x=r^{'}\cos(t)\\ y=r^{'}\sin(t)\\ z=c_1\end{cases} \tag{16}$$

where t is the simulation time, c is the position of the task plane along the z-axis, and $r^{'}$ is the trajectory's radius.

For this simulation, the test time is set as 8 s, and the other structural parameters of the proposed mechanism are set out in Table 1. The results are provided in Figure 4-7. Figure 4 and 5 show the desired and actual lengths of the three driving joints. The different color lines are the three prismatic joints l_1, l_2, and l_3. The desired results are calculated by the inverse kinematics, and the actual results are obtained by simulation. We observed that the desired and actual trends of the joints are similar, and the error between them is shown in Figure 6. The scale of the error between the desired and actual lengths is only 10^{-5}, which is far less than the scale of the desired or actual length. Figure 7 is the desired and actual trajectories of the end-effector. The differences between the desired and actual trajectories are caused by the initial parameters. Thus, the inverse kinematics for the parallel section are validated.

Table 1 The parameter of the mechanism

Parameter	Value	Parameter	Value
c	0.0375m	θ	56°
d	0.150m	a	0.0335m
r	0.0224m	c_1	0.130m
r_2	0.050m	$r^{'}$	0.02m

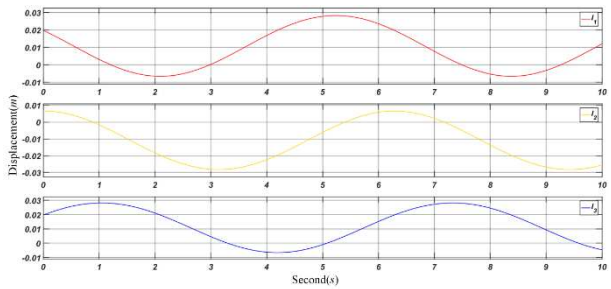

Figure 4 Desired lengths of the prismatic joints

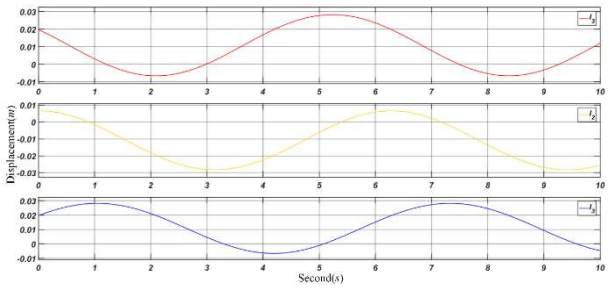

Figure 5 Actual lengths of the prismatic joints

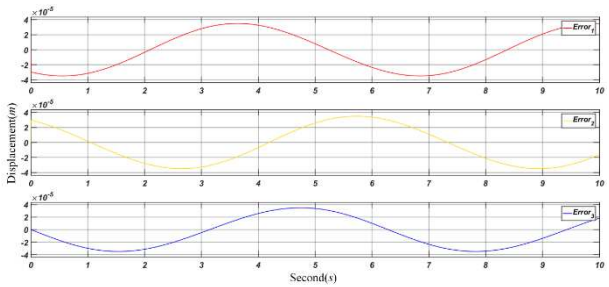

Figure 6 Error between actual and desired lengths

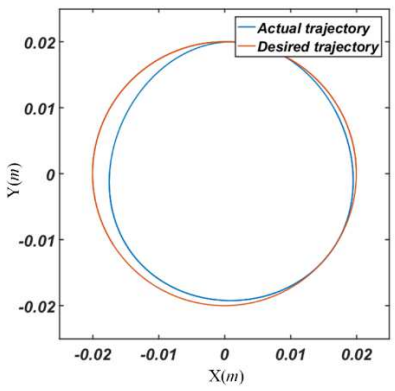

Figure 7 A comparison between actual and desired trajectories

3.2 Jacobian matrix and its applications

The proposed mechanism has three DOFs, but it is actuated by four actuators. When the proposed mechanism is in its regular working condition, the reconfigurable platform is fixed - i.e., the reconfigurable parallel mechanism only has three input parameters (three prismatic joints) and three output parameters translated along the 3 coordinate axes. Thus, the Jacobian matrix of this reconfigurable parallel mechanism is written as:

$$\mathbf{f}(\mathbf{x},\mathbf{q}) = 0 \tag{17}$$

The vector equation for this mechanism was obtained in Eq. (9). By deriving Eq. (9), the relationship between the driving joints and the translations of the end-effector is obtained as follows:

$$J_x \dot{\mathbf{x}} = J_q \dot{\mathbf{q}} \tag{18}$$

where $\dot{\mathbf{x}} = \begin{bmatrix} \dot{x} & \dot{y} & \dot{z} \end{bmatrix}^{\mathbf{T}}$ and $\dot{\mathbf{q}} = \begin{bmatrix} \dot{l}_1 & \dot{l}_2 & \dot{l}_3 \end{bmatrix}^{\mathbf{T}}$.

In this paper, J_x and J_q can be calculated according to the constraint equations of the three limbs. Thus, the Jacobian matrix is given as:

$$J = J_q^{-1} \cdot J_x \tag{19}$$

Then, the relationship between the input and output parameters is calculated.

According to the Jacobian matrix, the dexterity and stiffness of the proposed mechanism located at a specific position is calculated.

When this reconfigurable section is locked, the stiffness model for the parallel section located at a certain position is written as:

$$\boldsymbol{\kappa} = \mathbf{J}^{\mathrm{T}} \boldsymbol{\kappa}_{\mathbf{J}} \mathbf{J} \tag{20}$$

where $\boldsymbol{\kappa}_{\mathbf{J}}$ is the joint stiffness matrix, with $\boldsymbol{\kappa}_{\mathbf{J}} = diag\left[h_1, h_2, h_3\right]$.

Based on the Jacobian matrix, the relationship between the accuracy of the moving platform and the errors on the actuators, namely, dexterity, can be calculated as:

$$\kappa = \sqrt{\frac{\lambda_{\max}}{\lambda_{\min}}} \tag{21}$$

where $\lambda_{\max}$ and $\lambda_{\min}$ are the largest and smallest eigenvalues of the stiffness matrix.

The proposed mechanism has three same limbs, in this case, $h_1 = h_2 = h_3$. In this section, assuming $h_1 = 100\,\mathrm{KN/m}$, $z = 300\,\mathrm{mm}$, and $\theta = 56°$, Figure 8 shows the mapping figures of the stiffness and dexterity. It shows that stiffness is at its best when the moving platform is located in the central area, and its stiffness is nonlinearly decreasing at the edge of the reachable area. We can see that the stiffness map is of a central symmetry, which is consistent with the

structure of the proposed mechanism. The dexterity for the mechanism is shown in Figure 8 (c and d) – it is similar to the stiffness analysis. This mechanism shows the best dexterity when it is near the central area, and it possesses the worst dexterity when it is moving near the workspace's boundary position. The shape of the dexterity is symmetrical as well.

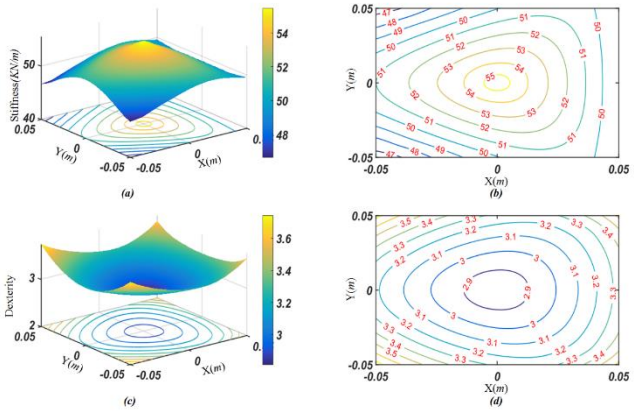

Figure 8 Stiffness and dexterity: (a) stiffness, (b) contour line for stiffness, (c) dexterity, (d) contour line for dexterity

3.3 Kinematics performance

The workspace is the reachable area of the moving platform in the fixed coordinate system, and the proposed mechanism only has three translational DOFs.

There are several constraints for the workspace of a mechanism, such as the geometrical parameters of the link or platform, the interference between links or platforms, etc. Here are the constraints for the mechanism proposed in this paper:

$$20\text{mm} \le l_i \le 150\text{mm} \tag{22}$$

In order to avoid interference between links or platforms, some constraints are proposed. As shown in Figure 9, the angle between two passive links, β, should be given a suitable range to avoid any collisions among components. Thus, the constraint can be given as:

$$\theta \le \beta \le \frac{\pi}{2} \tag{23}$$

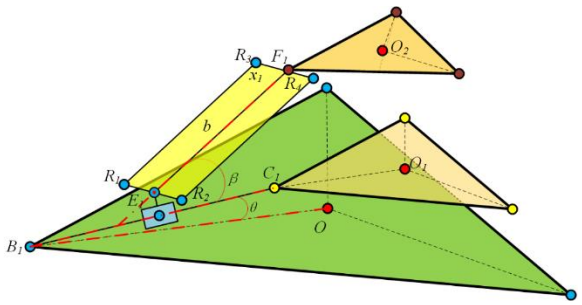

Figure 9 The angle constraint for the workspace

Based on the structural parameters, angle β can be calculated as:

$$\beta = \arccos\left(\frac{\overrightarrow{E_1F_1}\cdot\overrightarrow{B_1C_1}}{\left\|\overrightarrow{E_1F_1}\right\|\cdot\left\|\overrightarrow{B_1C_1}\right\|}\right) \tag{24}$$

According to the condition, the workspace of the reconfigurable parallel mechanism is located at two, limited configurations (Figure 10). Figure 10 shows the workspace in different conditions. The black, green, and red lines represent the fixed, middle, and moving platforms, respectively, and the dashed line is the z-axis. According to the structural parameters, the minimum and maximum angles, θ, are 55° and 75°, respectively. Thus, the configurations are the two limited positions for the reconfigurable mechanism when $\theta = 55°$ and $\theta = 75°$. Figure 10 (a and c) shows the comparisons between the size of mechanism and the shape of the workspace, and Figure 10 (b and d) illustrates the xoy projection while this mechanism is located in different configurations. When the angle increases, the ratio between the area of the maximum xoy projection and the area of the fixed platform increases.

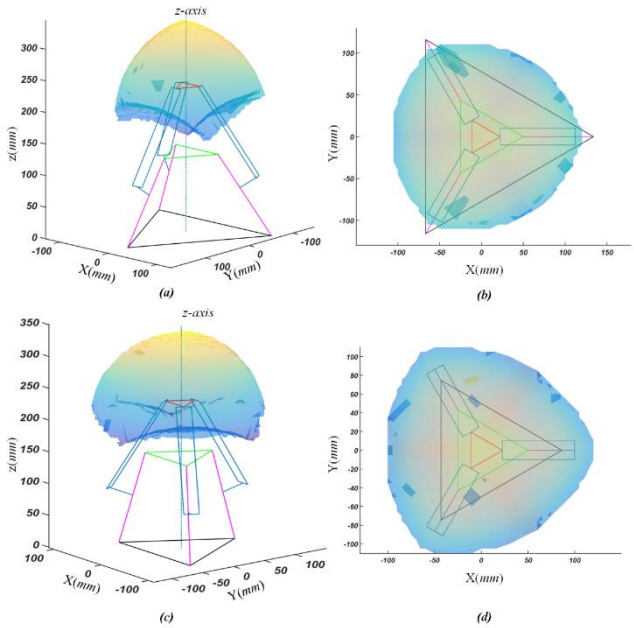

Figure 10 The workspace when the mechanism is located at the two limited positions: (a) $\theta = 55°$, (b) the xoy projection when $\theta = 55°$, (c) $\theta = 75°$, (d) the xoy projection when $\theta = 75°$

In this paper, a performance index is defined by the ratio between the areas of the maximum xoy projection and the area of the fixed platform, which is called the Area Ratio (AR). When the AR is larger, the mechanism has a better workspace, because it has a larger workspace to complete the task. It can be calculated as:

$$AR = \frac{\square\left(\max\left(xoy\right)\right)}{\square B_1B_2B_3} \tag{25}$$

Based on the AR, dexterity, and stiffness, the performance information can be found when the mechanism is in different configurations. In order to unify the units of these indices, some equations are

$$Dexterity\ Ratio(DR) = \frac{mean(Dexterity(\theta_i))}{mean(Dexterity(\theta_1))} \tag{26}$$

$$Stiffness\ Ratio(SR) = \frac{mean(Stiffness(\theta_i))}{mean(Stiffness(\theta_1))} \tag{27}$$

These equations are the ratios between the mean dexterity or stiffness of different configurations and the initial position. For the mechanism discussed in this paper, the variation trend is shown in Figure 11. When the angle becomes larger, AR becomes better, and DR and SR become worse. Figure 11 shows the changes in performance in the reconfigurable, parallel mechanism when the proposed mechanism is in different configurations.

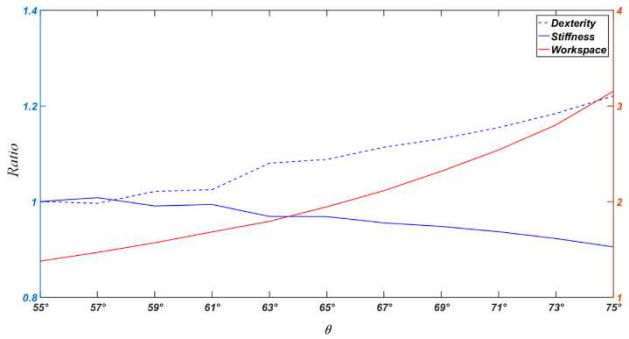

Figure 11 Trends of performance indices

4 Dynamics analysis

4.1 Dynamics analysis of the reconfigurable section

For the reconfigurable part, according to virtual work theory, the dynamics equation is written as:

$$\left(-m_w\mathbf{a} - m_wg\mathbf{e}\right)^{\mathrm{T}}\delta z_r + \left(\mathbf{F_r} - m_h\mathbf{a_m}\right)\delta m = 0 \tag{28}$$

where $\mathbf{e} = \begin{bmatrix}0 & 0 & 1\end{bmatrix}^{\mathrm{T}}$; m_w is the total mass consists of parallel section and the equivalence mass for the identical limbs, $B_iC_i(i=1,2,3)$; $\mathbf{F_r}$ is the force of the actuator; m_h is the total mass including the sliders and the equivalence mass for the identical limbs, $B_iC_i(i=1,2,3)$.

The relationship between δz_r and δm can be calculated from the Jacobian matrix. Thus, according to the kinematics equation of the reconfigurable section, differentiating Eq. (7) with respect to time, thus yields:

$$\dot{z}_r = \dot{\theta} \times \overrightarrow{B_iC_i} + \dot{m} \tag{29}$$

Similarly to the reconfigurable section, the Jacobian matrix can be written as:

$$\dot{z}_r = J_r\dot{m} \tag{30}$$

where $J_r = \dfrac{\sqrt{d^2 - \left(m - r_2\right)^2}}{m - r_2}$.

Thus,

$$\delta z_r = J_r\delta m \tag{31}$$

Substituting Eq. (31) to Eq. (28), yields:

$$\mathbf{F_r} = \frac{\left(m_w\mathbf{a} + m_wg\mathbf{e}\right)^{\mathrm{T}}}{J_r} + m_h\mathbf{a_m} \tag{32}$$

4.2 Inverse dynamics analysis for the parallel section

In this part, the inverse dynamic model for the parallel mechanism is established using Lagrange Theory. For this section, there are three redundant coordinates, x, y and z - when using this method's first type - and the generalized coordinates are set as x, y, z, l_1, l_2, and l_3.

The first type of equation is written as:

$$\frac{d}{dt}\left(\frac{\partial L}{\partial \dot{q}_j}\right) - \frac{\partial L}{\partial q_j} = Q_j + \sum_{i=1}^{k}\lambda_i\frac{\partial \Gamma_i}{\partial q_j}(j = 1\cdots 6) \tag{33}$$

where Γ_i denotes the *ith* constraint function, k is the number of constraint functions, and λ_i is the Lagrange multiplier. The six variables are $\lambda_i(i=1,2,3)$, and the three actuator torques are $Q_j(j=4,5,6)$. $Q_i(i=1,2,3)$ represent the x, y, and z components of an external force exerted on the moving platform.

In this case, Eq. (33) can be written as two sets. The first set considers the Lagrange multipliers as the only unknowns that can be written as:

$$\sum_{i=1}^{k}\lambda_i\frac{\partial \Gamma_i}{\partial q_j} = \frac{d}{dt}\left(\frac{\partial L}{\partial \dot{q}_j}\right) - \frac{\partial L}{\partial q_j} - \hat{Q}_j \tag{34}$$

where $\hat{Q}_j$ represents the external force exerted on the moving platform, Γ_i is the ith limb's constraint equation,

and L represents the total energy of the proposed mechanism.

To simplify the dynamics analysis, we assume that the mass of the identical length link, is divided to the endpoints of the limb. The energy of the proposed mechanism is given as:

$$L=\frac{1}{2}m_p(\dot{x}^2+\dot{y}^2+\dot{z}^2)+\frac{3}{2}m_b(\dot{x}^2+\dot{y}^2+\dot{z}^2)+\frac{1}{2}(m_a+m_b)(\dot{l}_1^2+\dot{l}_2^2+\dot{l}_3^2)-(3m_b+m_p)zg-\sum_{i=1}^{k}(m_b+m_a^i)l_i g\sin(\theta) \tag{35}$$

where m_p is the mass of the moving platform and m_s^i is the mass of the slider in the ith limb.

The formulation requires three constraint equations, $\Gamma_i(i=1,2,3)$. The distance between joints E_i and F_i is equal to the length of the virtual link b

$$\Gamma_i=\left\|\overrightarrow{E_iF_i}\right\|^2-b^2=0(i=1,2,3) \tag{36}$$

Then, substituting Eqs. (35) and (36) into Eq. (34), the Lagrange multiplier, λ_i, can be calculated. Once the Lagrange multipliers are found, the driving forces are determined directly by the second type of equation. Thus, we obtain:

$$F_j=\frac{d}{dt}(\frac{\partial L}{\partial \dot{q}_j})-\frac{\partial L}{\partial \dot{q}_j}-\sum_{i=1}^{k}\lambda_i\frac{\partial \Gamma_j}{\partial q_j}(j=1,2,3) \tag{37}$$

and the forces of the driving joints can be calculated.

4.3 Numerical example

To illustrate the dynamics analysis, consider the trajectory of the manipulator along the Archimedean spiral. In this spiral, the velocity of the end-effector is uniform. The trajectory of the end-effector can be given as:

$$\begin{aligned} r_d&=c_1(c_2+t)\\ x&=r_d\cos(t)\\ y&=r_d\sin(t)\\ z&=c_d \end{aligned} \tag{38}$$

where c_1 and c_2 are the constants of the spiral; c_d is the location of this plane.

To calculate the driving forces of the three joints, some initial parameters should be given. In this section, the external force of the moving platform is $[0\ \ 0\ \ 0]^{\mathrm{T}}$, $c_1=0.01\mathrm{m/s}$, $c_2=0.1\mathrm{s}$, $c_d=0.23\mathrm{m}$, and Table 2 shows the other design parameters. The driving forces are shown in Figure 12 and 13. The forces of the three joints increase gradually, and there are no cusps in Figure 12. The trajectory of the end-effector fits this given Archimedean spiral.

Table 2 Parameters of the reconfigurable parallel mechanism

Parameter	Value	Parameter	Value
c	0.0375m	θ	57°
d	0.15m	r_c	0.15m
r	0.02243m	m_b	0.0084Kg
r_2	0.05m	m_p	0.0649Kg
a	0.0335m	m_a	0.0481Kg
b	0.1645m	g	9.8Kg/s^2

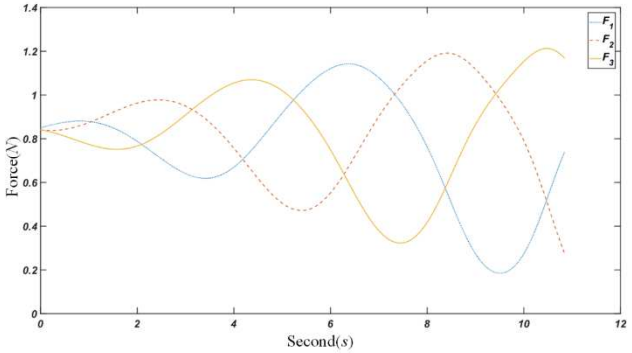

Figure 12 The forces of the three driving joints

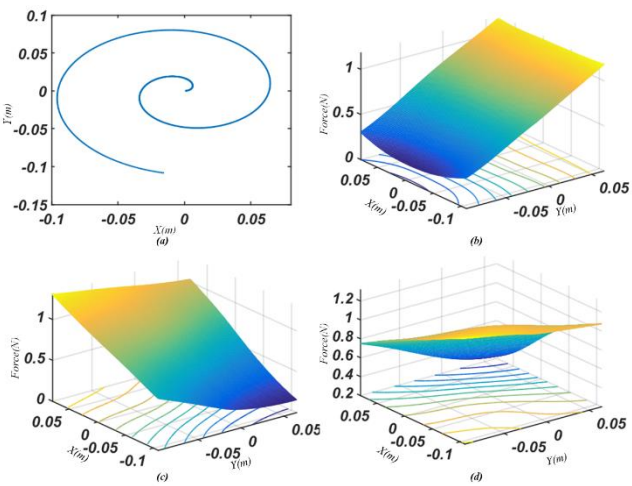

Figure 13 The results of the numerical example: (a) the trajectory of the moving platform, (b) the mapping of F_1, (c) the mapping of F_2, (d) the mapping of F_3

4.4 Dynamics performance

In this part, a novel dynamics performance is proposed using Lagrangian method. The driving forces of the actuators are calculated by Eq. (37), and the dynamic model is written as the matrix formulation, which is:

$$\mathbf{F}=\mathbf{C}-\boldsymbol{\lambda}\cdot\mathbf{D} \tag{39}$$

where $\mathbf{C}=\left[\frac{d}{dt}(\frac{\partial L}{\partial \dot{q}_j})-\frac{\partial L}{\partial \dot{q}_j}\right]^{\mathrm{T}}(j=4,5,6)$; $\boldsymbol{\lambda}=[\lambda_1\ \ \lambda_2\ \ \lambda_3]^{\mathrm{T}}$;

$\mathbf{D}=\left[\frac{\partial \Gamma_j}{\partial q_j}\right]^{\mathrm{T}}$ $(j=4,5,6)$.

Based on Eq. (34), the Lagrange multipliers can be written as the matrix formulation, which is:

$$\boldsymbol{\lambda}=\mathbf{A}^{-1}\mathbf{B} \tag{40}$$

where

$\mathbf{A}=\left[\frac{\partial \Gamma_i}{\partial q_j}\right]^{\mathrm{T}}$ $(j=1,2,3)$ $\mathbf{B}=\left[\frac{d}{dt}\left(\frac{\partial L}{\partial \dot{q}_j}\right)-\frac{\partial L}{\partial q_j}-\hat{Q}_j\right]^{\mathrm{T}}$ $(j=1,2,3)$.

Substituting Eq. (40) into Eq. (39), we get:

$$\mathbf{F}=\mathbf{C}-\mathbf{E}\mathbf{D} \tag{41}$$

where $\mathbf{E}=\mathbf{A}^{-1}\mathbf{B}$

The elements in the matrices $\mathbf{C}$ and $\mathbf{B}$ are known. The driving forces are determined with matrix $\mathbf{E}$.

The driving forces are indirectly related to the eigenvalues of $\mathbf{E}$. In this case, the dynamics index can be expressed by the eigenvalues of matrix $\mathbf{E}$. When $z=0.23\mathrm{m}$, the dynamics index is shown in Figure 14. Figure 14(a, b, and c) shows the eigenvalue mappings of the three eigenvalues for the matrix, and (d) illustrates the variance of these eigenvalues.

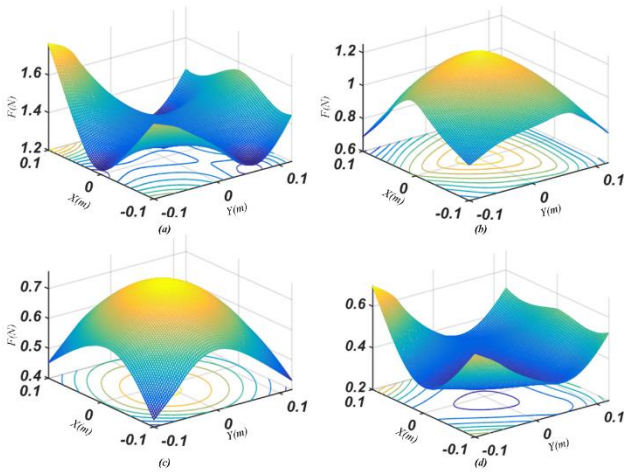

Figure 14 The dynamic indices: (a) the first eigenvalue, (b) the second eigenvalue, (c) the third eigenvalue, (d) the variance of these eigenvalues

5 Optimization

The proposed reconfigurable parallel mechanism is able to change the structural parameters to obtain different dynamic performance. When the reconfigurable section is located at a certain configuration, this mechanism will be locked.

5.1 Performance criterion

The AR is an index that evaluates comprehensive workspace performance. If the AR is larger, the mechanism has a better workspace. Meanwhile, the VDM is the fluctuation index of the driving forces given by the actuators. If the VDM is small, the mechanism will have a better dynamic performance.

5.2 Optimization and results

In this paper, the Multi-Objective Genetic Algorithm (MOGA) is used to optimize the kinematic and dynamic performance of the reconfigurable parallel mechanism. Table 3 lists the parameters of the initial optimization condition, and the optimal parameters are set as: population=20, array element=7, crossover probability=0.9, mutation probability=0.05. The optimization generation is set as 30. The detailed optimization process of a multi-objective performances with a Pareto-based MOGA is presented in Figure 15. Figure 15 (a) shows the convergence of the two objective functions, and the blue line is the variable trend of the AR; the red line is the trend for the VDM. After the 15th generation, the trends for both the AR and VDM became stable. Compared with the initial performance, the AR is improved from 0.705 to 0.8418 (an increase of 19.4%), and the VDM is reduced from 0.338 to 0.282 (a reduction of 16.5%). Figure 15 (b) is the optimization results of the Pareto frontier. Figure 15 (c) illustrates the changes of all individuals in the 30th generation. After the optimization, the performance is greatly improved.

In order to choose the best solution in the solution, a comprehensive index (CI) is selected to evaluate the results' performance. In this paper, the units of two performance indices are identical, and so the CI can written as

$$CI=AR+VDM \tag{42}$$

Based on the MGOA and CI, the final results are listed in Table 4, and the best solution is marked in bold - i.e., the 19th set. In Figure 16 (a), the red line is the average of the CI, and the blue line is the CI values of each set. Figure 16 (b) illustrates the distance between the average and the value of each set, and the best solution is marked by the red circle in Figure 16. The 3D prototype is shown in Figure 16. Figure 17 (a) shows the spatial multi-loop over-constrained mechanism, while Figures. 15 (b, c, and d) illustrate the different configurations.

Table 3 Variable range

Variable	Range(m)	Variable	Range(m)
r	0.02~0.04	a	0.03~0.05
b	0.15~0.18		

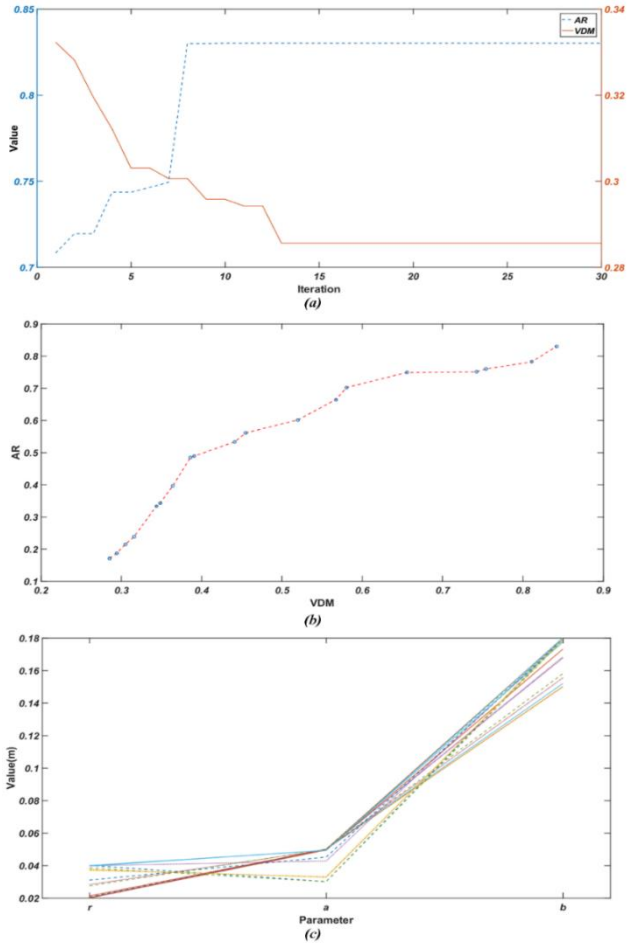

Figure 15 Multi-objective optimization results: (a) convergence of objective function, (b) Pareto frontier, (c) trends of the optimized variables

Table 4 The results of the optimization

r/m	*a*/m	*b*/m	*VDM*	*AR*	*Distance*
0.0400	0.0301	0.1800	0.8418	0.8300	0.6896
0.0200	0.0500	0.1500	0.2856	0.1707	0.5259
0.0200	0.0500	0.1500	0.2856	0.1707	0.5259
0.0200	0.0500	0.1677	0.3437	0.3333	0.3053
0.0202	0.0500	0.1580	0.3158	0.2380	0.4284
0.0200	0.0500	0.1519	0.2943	0.1870	0.5010
0.0200	0.0500	0.1554	0.3050	0.2142	0.4631
0.0310	0.0452	0.1788	0.5197	0.6009	0.1384
0.0200	0.0495	0.1731	0.3641	0.3967	0.2214
0.0371	0.0330	0.1790	0.7420	0.7506	0.5104
0.0398	0.0427	0.1800	0.6554	0.7486	0.4218
0.0385	0.0300	0.1787	0.8110	0.7818	0.6105
0.0396	0.0494	0.1775	0.5670	0.6641	0.2490
0.0282	0.0496	0.1800	0.4549	0.5611	0.0338
0.0206	0.0500	0.1800	0.3860	0.4843	0.1120
0.0212	0.0500	0.1800	0.3909	0.4889	0.1024
0.0375	0.0327	0.1790	0.7538	0.7594	0.5310
0.0204	0.0500	0.1683	0.3483	0.3424	0.2915
0.0275	**0.0499**	**0.1789**	**0.4413**	**0.5331**	**0.0078**
0.0400	0.0492	0.1800	0.5805	0.7020	0.3002

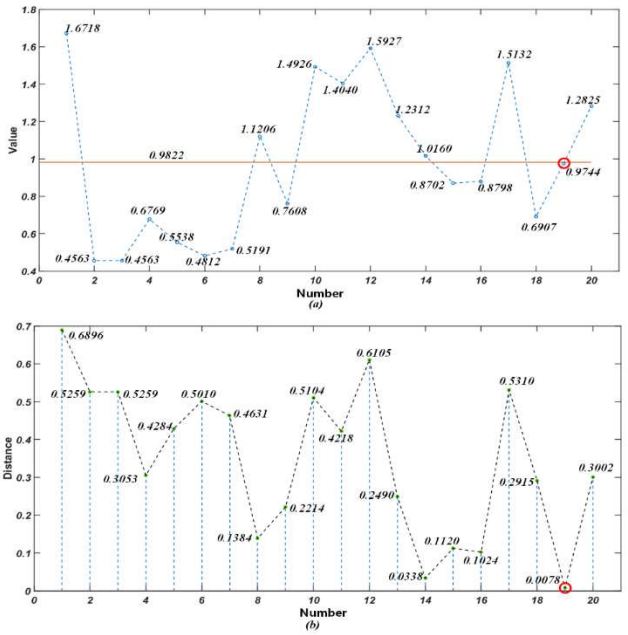

Figure 16 The *CI* index: (a) values of the sets, (b) distance between the average and the value

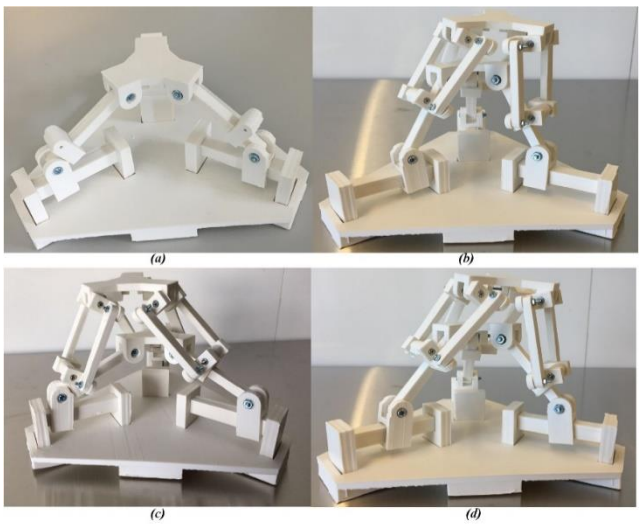

Figure 17 The 3D-printed model: (a) the spatial, multi-loop, over-constrained mechanism, (b) configuration Ⅰ, (c) configuration Ⅱ, (d) configuration Ⅲ

6 Conclusion

(1) A novel reconfigurable parallel mechanism is proposed, according to the spatial multi-loop over-constrained mechanism, which can change its configurations continuously. Using screw theory, the analysis of the mobility of the spatial over-constrained mechanism and reconfigurable parallel section is conducted. The inverse kinematics for the mechanism is obtained.

Some kinematic performance indices, such as dexterity and stiffness, are both analyzed. The workspace of the mechanism is calculated, and a new index is proposed - the Area Ratio (AR). The trends of the kinematic performance indices are illustrated when the reconfigurable section moved at different configurations.

(2) Based on the virtual work principal, the dynamics model of the reconfigurable section was obtained. Using the Lagrange theory, the dynamics analysis of the parallel section was calculated, and a numerical example is provided to verify the dynamics analysis. Meanwhile, a novel performance index is presented - the variance of dynamics matrix (VDM).

(3) The Area Ratio and the variance of dynamics matrix are considered as the objective functions, a multi-objective optimization is applied to achieve better structural parameters, and by applying the CI, the best structural parameters are selected from the optimized solutions. A new approach to select the suitable solution from the optimal results is introduced in this paper, and the kinematics and dynamics performance indices are generic and can be applied to optimize the other parallel mechanisms.

7 Declaration

Acknowledgements

The authors sincerely thanks to Professor Dan Zhang of York University for his critical discussion and reading during manuscript preparation.

Funding

The authors would like thank the Leading Innovation and Entrepreneurship Team of Zhejiang Province of China (Grant No. 2018R01006). The authors also would like to thank the financial support from the Natural Sciences and Engineering Research Council of Canada (NSERC) and gratefully acknowledge the financial support from the York Research Chairs (YRC) program.

Availability of data and materials

The datasets supporting the conclusions of this article are included within the article.

Authors' contributions

The author' contributions are as follows: Dan Zhang was in charge of the whole trial; Guan-Yu Huang wrote the manuscript; Qi Zou and Ling-Yu Kong assisted with sampling and laboratory analyses.

Competing interests

The authors declare no competing financial interests.

Consent for publication

Not applicable

Ethics approval and consent to participate

Not applicable

References

[1] G Huang, S Guo, D Zhang, et al. Kinematic analysis and multi-objective optimization of a new reconfigurable parallel mechanism with high stiffness[J]. *Robotica*, 2018,36(2):187-203.

[2] S A Moezi, M Rafeeyan, E Zakeri, et al. Simulation and experimental control of a 3-RPR parallel robot using optimal fuzzy controller and fast on/off solenoid valves based on the PWM wave[J]. *ISA Transactions*, 2016,61:265-286.

[3] G Coppola, D Zhang, K Liu. A 6-DOF reconfigurable hybrid parallel manipulator[J]. *Robotics and Computer-Integrated Manufacturing*, 2014,30(2):99-106.

[4] Y Tian, D Zhang, Y Yao, et al. A reconfigurable multi-mode mobile parallel robot[J]. *Mechanism and Machine Theory*, 2017,111:39-65.

[5] C Yang, J Zhao, L Li, et al. Design and implementation of a novel modal space active force control concept for spatial multi-DOF parallel robotic manipulators actuated by electrical actuators[J]. *ISA Transactions*, 2018,72:273-286.

[6] W Ye, Y Fang, K Zhang, et al. Mobility variation of a family of metamorphic parallel mechanisms with reconfigurable hybrid limbs[J]. *Robotics and Computer-Integrated Manufacturing*, 2016,41:145-162.

[7] L A Patrick, W M Arthur, J W Robert. Continuum Reconfigurable Parallel Robots for Surgery: Shape Sensing and State Estimation With Uncertainty[J]. *IEEE Robotics and Automation Letters*, 2017,2(3):1617-1624.

[8] Z Gao, D Zhang. Performance Analysis, Mapping and Multi-Objective Optimization of a Hybrid Robotic Machine Tool[J]. *IEEE Transactions on Industrial Electronics*, 2015,62(1):423-433.

[9] Q LI, L XU, Q CHEN, et al. New Family of RPR-Equivalent Parallel Mechanisms: Design and Application[J]. *Chinese Journal of Mechanical Engineering*, 2017,30(2):217-221.

[10] W Ye, Y Fang, K Zhang, et al. A new family of reconfigurable parallel mechanisms with diamond kinematotropic chain[J]. *Mechanism and Machine Theory*, 2014,74:1-9.

[11] W Ye, Y Fang, S Guo. Reconfigurable parallel mechanisms with planar five-bar metamorphic linkages[J]. *Science China Technological Sciences*, 2014,57(1):210-218.

[12] K Zhang, J S Dai. Screw-System-Variation Enabled Reconfiguration of the Bennett Plano-Spherical Hybrid Linkage and Its Evolved Parallel Mechanism[J]. *Journal of Mechanical Design*, 2015,137(6):62303.

[13] D Gan, J Dias, L Seneviratne. Unified kinematics and optimal design of a 3rRPS metamorphic parallel mechanism with a

reconfigurable revolute joint[J]. *Mechanism & Machine Theory*, 2015,96(2):239-254.

[14] D Gan, J S Dai, J Dias, et al. Reconfigurability and unified kinematics modeling of a 3rTPS metamorphic parallel mechanism with perpendicular constraint screws[J]. *Robotics and Computer-Integrated Manufacturing,* 2013,29(4):121-128.

[15] D Gan, J S Dai, J Dias, et al. Unified Kinematics and Singularity Analysis of a Metamorphic Parallel Mechanism With Bifurcated Motion[J]. *Journal of Mechanisms & Robotics*, 2013,5(3):1194-1227.

[16] D Zhang, Z Bi, B Li. Design and kinetostatic analysis of a new parallel manipulator[J]. *Robotics and Computer-Integrated Manufacturing*, 2009,25(4-5):782-791.

[17] X Zhang, X Zhang, Z Chen. Dynamic analysis of a 3-RRR parallel mechanism with multiple clearance joints[J]. *Mechanism and Machine Theory*, 2014,78:105-115.

[18] K Wisama, G Sylvain. Inverse and direct dynamic modeling of Gough-Stewart robots[J]. *IEEE Transactions on Robotics*, 2004,20(4):754-761.

[19] J Wu, J Wang, T Li, et al. Analysis and Application of a 2-DOF Planar Parallel Mechanism[J]. *Journal of Mechanical Design*, 2006,129(4):434-437.

[20] L Tsai. Robot analysis: the mechanics of serial and parallel manipulators[M]. John Wiley & Sons, 1999.

[21] S Staicu, D Zhang. A novel dynamic modelling approach for parallel mechanisms analysis[J]. *Robotics and Computer-Integrated Manufacturing*, 2008,24(1):167-172.

[22] S Staicu. Dynamics of the 6-6 Stewart parallel manipulator[J]. *Robotics and Computer-Integrated Manufacturing*, 2011,27(1):212-220.

[23] J Wu, X Chen, L Wang. Design and Dynamics of a Novel Solar Tracker With Parallel Mechanism[J]. *IEEE/ASME Transactions on Mechatronics*, 2016,21(1):88-97.

[24] J Wu, J Wang, L Wang, et al. Dynamics and control of a planar 3-DOF parallel manipulator with actuation redundancy[J]. *Mechanism and Machine Theory*, 2009,44(4):835-849.

[25] Y Zhao, F Gao, X Dong, et al. Dynamics analysis and characteristics of the 8-PSS flexible redundant parallel manipulator[J]. *Robotics and Computer-Integrated Manufacturing*, 2011,27(5):918-928.

[26] J Yao, W Gu, Z Feng, et al. Dynamic analysis and driving force optimization of a 5-DOF parallel manipulator with redundant actuation[J]. *Robotics and Computer-Integrated Manufacturing*, 2017,48:51-58.

[27] H Abdellatif, B Heimann. Computational efficient inverse dynamics of 6-DOF fully parallel manipulators by using the Lagrangian formalism[J]. *Mechanism and Machine Theory*, 2009,44(1):192-207.

[28] X Chen, L Wu, Y Deng, et al. Dynamic response analysis and chaos identification of 4-UPS-UPU flexible spatial parallel mechanism[J]. *Nonlinear Dynamics*, 2017,87(4):2311-2324.

[29] W Ye, X Chai, K Zhang. Kinematic modeling and optimization of a new reconfigurable parallel mechanism[J]. *Mechanism and Machine Theory*, 2020,149:103850.

[30] Z Gao, D Zhang. Performance Analysis, Mapping, and Multi-objective Optimization of a Hybrid Robotic Machine Tool[J]. *IEEE Transactions on Industrial Electronics*, 2015,62(1):423-433.

[31] Z Gao, D Zhang, Y Ge. Design optimization of a spatial six degree-of-freedom parallel manipulator based on artificial intelligence approaches[J]. *Robotics and Computer-Integrated Manufacturing*, 2010,26(2):180-189.

[32] S Jin, J Kim, T Seo. Optimization of a redundantly actuated 5R symmetrical parallel mechanism based on structural stiffness[J]. *Robotica*, 2015,33(09):1973-1983.

[33] X Liu, J Wang. A new methodology for optimal kinematic design of parallel mechanisms[J]. *Mechanism and Machine Theory*, 2007,42(9):1210-1224.

[34] Z Tao, Q An. Interference analysis and workspace optimization of 3-RRR spherical parallel mechanism[J]. *Mechanism and Machine Theory*, 2013,69:62-72.

[35] D Zhang, Z Gao. Forward kinematics, performance analysis, and multi-objective optimization of a bio-inspired parallel manipulator[J]. *Robotics and Computer-Integrated Manufacturing*, 2012,28(4):484-492.

[36] Q Zou, D Zhang, X Luo, et al. Enumeration and optimum design of a class of translational parallel mechanisms with prismatic and parallelogram joints[J]. *Mechanism and Machine Theory*, 2020,150:103846.

[37] Q Zou, D Zhang, S Zhang, et al. Kinematic and dynamic analysis of a 3-DOF parallel mechanism[J]. *International Journal of Mechanics and Materials in Design*, 2021,17(3):587-599.

Biographical notes

Guan-Yu Huang, born in 1989, is an assistant researcher in *Zhejiang Lab, China.* He received his Bachelor's and PhD degrees from *Beijing Jiaotong University* in 2013 and 2018 respectively. His research interests include design and control of parallel, biped and other robots.
E-mail: huanggy@zhejianglab.com

Dan Zhang, received his Ph.D. in Mechanical Engineering from *Laval University*, Canada, in June 2000. His research interests include robotics and mechatronics; high performance parallel robotic machine development; sustainable/green manufacturing systems; rehabilitation robot and rescue robot. Dr. Zhang's contributions to and leadership within the field of robotic and automation have been recognized with several prestigious awards, within his own university (Kaneff Professorship, Tier 1 York Research Chair in Advanced Robotics and Mechatronics, Research Excellence Award), the Province of Ontario (Early Researcher Award in 2010), the professional societies (Fellow of the Canadian Academy of Engineering, Fellow of the ASME, Fellow of the Engineering Institute of Canada and Fellow of the CSME, Senior Member of IEEE, Senior Member of SME), and federal funding agencies (Canada Research Chair in January 2009 and renewed in January 2014).
E-mail：dzhang99@yorku.ca

Qi Zou, received his Bachelor's and Master's degrees from *Beijing Jiaotong University* in 2016 and 2019, respectively. Currently he is a doctoral student in Mechanical Engineering at *York University*. His research interests contain design and performance analysis of parallel mechanism.
E-mail: qizou@yorku.ca

Ling-Yu Kong, born in 1988, is currently a researcher at

Intelligent Robot Research Center, Zhejiang Lab, Hangzhou, China. He received his PhD degree from *Shanghai Jiao Tong University*, China in 2018. His research interests include mechatronics engineering, robotics and manipulator calibration.
E-mail: kongly@zhejianglab.com